Available online at www.sciencedirect.com

ScienceDirect

journal homepage: www.elsevier.com/locate/he

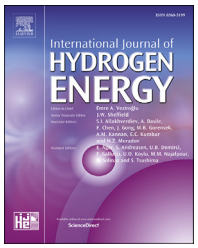

# Temperature-dependent dissolution and diffusion of H isotopes in iron for nuclear energy applications: First-principles and vibration spectrum predictions

*Qingyuan Chen* [a], *Qinglong Yao* [b], *Yue-Lin Liu* [a,*], *Quan-Fu Han* [c], *Fang Ding* [d]

[a] *Department of Physics, Yantai University, Yantai 264005, China*
[b] *College of Materials Science and Engineering, Jilin University, Changchun 130012, China*
[c] *Department of Physics, Beihang University, Beijing 100191, China*
[d] *Institute of Plasma Physics, Chinese Academy of Sciences, Hefei 230031, China*

ARTICLE INFO

*Article history:*
Received 9 December 2016
Accepted 18 February 2017
Available online 18 March 2017

*Keywords:*
Iron
Hydrogen dissolution and diffusion
Temperature and H chemical potential
First-principles
Vibration spectrum calculations

ABSTRACT

The dissolution and diffusion of H isotopes in bcc-Fe are fundamental and essential parameters in the H energy application from nuclear conversion, whereas the relevant data are lacking and relatively dispersive, demonstrating some important factors have been missed during the past studies. Here, we carry out first-principles total energy and vibration spectrum calculations to investigate systematically the interstitial H dissolution and diffusion behaviors in bcc-Fe by considering the temperature effect. Temperature and H chemical potential are two important factors to affect the H dissolution property. In the interstitial lattice, the H dissolution energy referring to the static/temperature-dependent H chemical potential decreases/increases with the increasing temperature. The diffusion activation energy and pre-factor of H also depend on the temperature and increase significantly with the increasing temperature from 300 to 1000 K. The temperature-correction can give a reasonable interpretation for the broad disseminating in the experimental data of H diffusivity in bcc-Fe. Our currently calculated results reveal that phonon vibration energy plays a crucial role in the H dissolution and diffusion with the increasing temperature.



## Introduction

As the presently significant example, the study of H-metal system has received particular attention because some metals might be considered as the structural material [1,2] or plasma facing material [3–5] in nuclear fusion energy application. Meanwhile, the structural material will suffer from different particles. In particular, under irradiation by the high energy neutrons (~14.1 MeV), large amounts of H atoms are produced via the transmutation reaction (*n*, *p*). This makes that H atoms

* *Corresponding author*. fax: +86 535 6902506.
E-mail address: liuyl@ytu.edu.cn (Y.-L. Liu).
http://dx.doi.org/10.1016/j.ijhydene.2017.02.133

can interact strongly with the lattice positions in structural material.

In nuclear energy application, the choice of the structural material is considered to be one of the key issues. The body centered cubic iron (bcc-Fe) is considered as a potential candidate of structural material. In the role of the structural material, bcc-Fe interacts with H atoms, which diffuse continuously and evolve in the bulk of bcc-Fe. The long retention of H atoms can result in the modification of physical and mechanical behaviors of bcc-Fe. For example, H can lead to the embrittlement, the decrease of mechanical strength and vacancy formation. Correspondingly, to gain the physical insight of the H behaviors in bcc-Fe is an extreme important work in the current fusion study. To study the H retention properties in bcc-Fe, we first determine the H dissolution energy and diffusion activation energy, owing to that the dissolution energy and diffusion activation energy of H are regarded as the input parameters to further obtain the dissolving concentration and diffusivity of H in bcc-Fe. In addition, the H solubility and diffusivity can also provide some effective references for the experimental researches of H behaviors in bcc-Fe.

Experimentally, there was little direct evidence to demonstrate the exact site occupancy of H in bcc-Fe because H exhibits the extremely low solubility, the relatively high mobility and the high probability of capturing by the defect positions at low temperatures [6]. While the indirect evidence hints that H might be located at the tetrahedral position in bcc-Fe [7]. More recently, using a relatively larger supercell with 128-Fe atom system, several simulation studies have addressed some relevant issues for the behaviors of H in bcc-Fe, including bulk dissolution energy and site occupancy, bulk diffusion process, vacancy trapping, interacting with dislocations and solutes, and influence of strain on the H capturing [8–17]. Their results consistently indicated that H prefers to occupy the tetrahedral position. Until now, the relevant data for the H dissolving concentration in bcc-Fe are relatively little, despite of that there were some results in both experimental and theoretical studies [7,18–22]. For example, Some earlier investigations on the H (as well as its isotope deuterium) solubility at temperature range from 300 to 1000 K have been carried out by Quick et al. [20] ($S(H/Fe)=(0.28-11.91)\times 10^{-3}\exp[-(0.293\pm 0.028)eV/kT]$, 555 K < $T$ < 1000 K), Hirth [7] ($S(H/Fe)=1.85\times 10^{-3}\exp(-0.295\ eV/kT)$), Sugimoto et al. [21] ($S(H/Fe)=0.82\times 10^{-2}\exp(-0.35\ eV/kT)$, 600 K < $T$ < 1000 K), and San-Martin et al. [22] (~$3.00\times 10^{-8}$(H/Fe) at $T$ = 300 K and ~$1.00\times 10^{-4}$(H/Fe) at $T$ = 1000 K).

Different from the H solubility in bcc-Fe, the existing data for the H diffusion including diffusion coefficient and activation energy in the interstitial lattice are not very scarce. Until now, there are some experimental and theoretical studies to determine the H diffusion coefficient and activation energy in bcc-Fe. Experimentally, the extensive investigations of H diffusion have been performed in different structural irons and steels [23–25]. In the earlier studies, nearly fifty research group results of the H diffusion in bcc-Fe were summarized by Völkl et al. [23] over the whole considered temperature regime of 300–1000 K. Experimentally, the typical activation energy changes from 0.035 to 0.142 eV and the diffusion pre-factor alters from $0.34\times 10^{-8}$ to $2.20\times 10^{-8}$ m$^2$/s. Theoretically, Several simulation studies also presented the H diffusion behavior in bcc-Fe and provided the diffusion data including pre-factor and activation energy, which were performed by Jiang et al. [10] ($1.50\times 10^{-7}\exp(-0.088\ eV/kT)$ m$^2$/s without zero-point-energy correction and $4.40\times 10^{-8}\exp(-0.043\ eV/kT)$ m$^2$/s with zero-point-energy correction), Sanchez et al. [11] ($1.00\times 10^{-8}\exp(-0.07\ eV/kT)$ m$^2$/s), Hayward [17] ($D=4.05\times 10^{-8}\exp(-0.04\ eV/kT)$ m$^2$/s), and Stefano et al. [26] ($1.00\times 10^{-8}\exp(-0.046\ eV/kT)$ m$^2$/s). Based on these theoretical calculations, the H diffusion pre-factor might go into the order of magnitude of ~$10^{-8}$–~$10^{-7}$ m$^2$/s, while the H diffusion activation energy should fall into the range of 0.04–0.09 eV. Thus, in both experiments and simulations, the diffusion equation of H in the interstitial lattice position in bcc-Fe might be expected to be $D$=(~$10^{-8}$–~$10^{-7}$)$\exp[-(0.03-0.14)eV/kT]$ m$^2$/s.

As mentioned above, although different data for the solubility and diffusivity of H in bcc-Fe have been partly given, there are still some questions to be addressed, especially those which concern the interaction of H with interstitial lattice position with the increasing temperature. For example, some researchers have indeed provided the relevant results from individual experimental measurements or computational simulations, but these experimental or theoretical results are not straightforward because only the temperature-independent pre-factor and activation energy are employed to analyze the experimental measurements or theoretical simulations so that Arrhenius-like behaviors of the solubility and diffusivity of H with the increasing temperature are not completely convincing in experimental and theoretical analyses. This means that the temperature-correction has been missed for the thermal activation process in previously most studies. On the other hand, the vibrational spectrum will also alter with the increasing temperature in bcc-Fe (as well as other metal), correspondingly the vibrational free energy related to the temperature will have a large effect on the solubility and diffusion of H in bcc-Fe. Additionally, we know that H in bcc-Fe as well as other transition metals exhibits the extremely low solubility, thus some experimental conditions such as the surface absorption, impurity and defect capturing influences could make the experimental examinations become relatively hard and complicated, especially at lower temperature case. All these factors can lead to that it is very difficult to obtain the valuable parameters for the solubility and diffusivity of H in bcc-Fe so that the reliable results will be urgently given.

As an effective simulation tool, first-principles method has been applied to study the impurity-metal system. It is well known that the behaviors of impurity in real materials is related to the temperature, which is certainly beyond the scope of the "simple" first-principles simulation. The temperature-correction should be an important omission because it has been suggested to be considered as a potential factor for explaining experimental dissolution and diffusion, but was not considered in the theoretical investigations previously [10,11,17,26]. Thus, how to predict the real properties of impurity in metals by combining the first-principles calculation with temperature is a key problem to interpret experiments. According to the previously reported results [27], bcc-Fe as well as other metals exhibits the

corresponding thermal expansion with the increase of temperature. For instance, the thermal expansion of bcc-Fe [27] was shown to be ~0.80% and ~1.27% for the temperature at $T = 600$ and 900 K, respectively. In addition, Matsumoto et al. [12] recently investigated the effect of strain (tensile or compressive strain) on H dissolution energy in bcc-Fe using first-principles simulation. Their results have indicated that the strain, i.e., the volume expansion or compression, can effectively alter the dissolution energy of H in bcc-Fe. At the same time, Li et al. [28] presented that the lattice compression or expansion can also cause the alteration of H diffusion activation energy in tungsten. As mentioned above, the increase of temperature leads to the alteration of vibrational spectrum in metal, which can directly affect the total energy of impurity-metal system. Therefore, the temperature should be expected to have a large influence on the dissolution and diffusion of H in bcc-Fe. For instance, how is the H dissolution energy affected by the temperature? i.e., how does the H solution energy changes with the increasing temperature? This is the first question that we need to solve in the current study. The H dissolving concentration in metals can be generally determined by the "temperature-independent" dissolution energy obtained using first-principles ground-state prediction in most previously studies. Correspondingly, the calculated H dissolving concentration comparing with the experimental data is not convincing since the temperature-dependent H dissolution energy has been not provided in previous calculations. Therefore, how does the H dissolving concentration alters with the increasing temperature if the temperature-dependent dissolution energy is used as an input parameter in bcc-Fe? This is the second question that we need to answer in this work. Further, how is the H diffusion activation energy influenced by the temperature? In most previously calculations, all atomic nuclei are treated as point-like classical particles which can lead to inaccuracies in the description of H diffusion activation energy, since the temperature effect has been negligible. Thus, the third question is to clarify the effect of temperature on the diffusion activation energy of H in bcc-Fe.

Motivated by the above questions, in this work we have performed systematically first-principles total energy and vibrational spectrum calculations to determine the dissolution and diffusion of H in the interstitial lattice position at finite temperature in bcc-Fe. We demonstrate that, although H in perfect bcc-Fe always prefers to occupy the tetrahedral lattice position and its diffusion route is mainly along the nearest neighbor tetrahedral lattice sites over the whole considered temperature range of 300–1000 K, the temperature is found to have a large influence on the dissolution and diffusion of H in bcc-Fe. With the increasing temperature, two cases occurring to the H dissolution energy in bcc-Fe. The H dissolution energy decreases/increases with the increasing temperature, if the static/temperature-dependent H chemical potential is chosen as energy reference. Also, the H diffusion activation energy is strongly dependent on the temperature and increases with the increasing temperature.

## Methodology

### *Total energy calculations of H-bcc-Fe system*

For all the energy calculations, we carried out first-principles simulations using the Vienna Ab-initio Simulation Package (VASP) code [29,30] based on density functional theory (DFT). The electron exchange and correlation were treated within the generalized gradient approximation (GGA) using the Perdew-Burke-Ernzerh of functional [31–33]. The ionic cores were represented by the projector augmented wave potentials [34,35]. As a typical magnetic transition metal, the spin polarization has been taken into account for bcc-Fe [36]. The energy cutoff of plane wave is 350 eV, which is sufficient for the total energy and geometry of Fe supercell with and without H impurity. During the geometry optimization, we used the 250-atom supercell containing ($5 \times 5 \times 5$) unit cells with the lengths of 14.25 Å in the [100], [010], and [001] directions, respectively. Table 1 shows the results of convergence testing for the 250-atom supercell size. The calculated equilibrium lattice constants are 2.85 Å, which is in good agreement with the corresponding experimental values of 2.87 Å [37]. The Brillouin zone of supercell was sampled with the Monkhorst–Pack scheme [40] using a ($2 \times 2 \times 2$) $k$-points mesh. The Methfessel-Paxton [41] smearing method was used to integrate the Brillouin zone and account for partial occupancies of the metals near the Fermi level with a smearing width of 0.1 eV. During the calculations, the supercell size and

**Table 1 – Results of convergence testing for the 250-atom supercell size. Lattice constant $a_0$ (Å), bulk modulus $B_0$ (GPa), and magnetic moment $\mu_0$ ($\mu_B$ per Fe atom) of the perfect bcc-Fe including the current calculations and other results of calculations and experiments. We also give the dissolution energies $G_H^d$ (eV) of the tetrahedral interstitial H with and without zero-point energy (ZPE), respectively, and ZPEs (eV) of interstitial H and an $H_2$ molecule in vacuum, respectively.**

| Property | Other simulations | This work | Expt. |
|---|---|---|---|
| $a_0$ | 2.86[a], 2.85[b], 2.83[c], 2.87[d] | 2.85 | 2.87[e] |
| $B_0$ | 155[a], 152[b], 174[c] | 153 | 168[e] |
| $\mu_0$ | 2.32[a], 2.24[b], 2.20[c] | 2.21 | 2.22[e] |
| $G_H^d$ (without-ZPE) | 0.20[c], 0.13[g] | 0.19 | |
| $G_H^d$ (with-ZPE) | 0.30[c], 0.32[b], 0.23[g] | 0.31 | 0.29[f], 0.296[h] |
| ZPE of interstitial H | 0.234[c], 0.261[d], 0.240[g] | 0.25 | |
| ZPE of $H_2$ | 0.133[c], 0.140[g] | 0.135 | 0.136[i], 0.137[j] |

[a] Ref. [26].
[b] Ref. [9].
[c] Ref. [10].
[d] Ref. [26].
[e] Ref. [37].
[f] Ref. [38].
[g] Ref. [17].
[h] Ref. [7].
[i] Ref. [39].
[j] Ref. [39].

atomic positions are relaxed to equilibrium, and energy minimization is converged until the forces on all the atoms are less than $10^{-3}$ eVÅ$^{-1}$.

### *Calculations of dissolution energy and dissolving concentration of H in bcc-Fe: thermodynamic and statistical model*

The dissolution energy of H in the interstitial lattice at finite temperature is attributed to the variation of the Gibbs free energy at temperature $T$ and pressure $P$ [42],

$$G_H^d(T,P) = G_{H-Fe}(T,P) - G_{Fe}(T,P) - \mu_H(T,P), \quad (1)$$

where $G_{H-Fe}(T,P)$ and $G_{Fe}(T,P)$ are, respectively, the Gibbs free energies of one H-Fe and perfect Fe systems at temperature $T$ and pressure $P$, and they are given as

$$G(T,P) = E_{a_T} + F_{a_T}^{vib}(T) + pV(T,P) - TS^{conf}, \quad (2)$$

where $E_{a_T}$ is the DFT static energy at $T = 0$ K, which is calculated from the current first-principles simulation as the ground-state energy at a given lattice constant $a_T$. As to the lattice constant $a_T$, it will increase with the increasing temperature (see the explanation in the last paragraph of the Methodology section). The term $PV$ can be neglected for solid state systems [42]. $S^{conf}$ is the configurational entropy which is expressed as $S^{conf} = k \ln Z_i^{conf}$, where $Z_i^{conf}$ is the number of configurations for an interstitial H atom in perfect bcc-Fe. As interstitial lattice, we assume that there are $l$ sites *per* Fe atom for H and the number of H atoms in an interstitial site is $n_{H_i}$, accordingly the number of configurations for H in interstitial positions is given as $Z_i^{conf} = \frac{l!}{n_{H_i}!(l-n_{H_i})!}$. $F_{a_T}^{vib}(T)$ is the vibrational Helmholtz free energy [42] and in the quasi-harmonic approximation it is written as

$$F_{a_T}^{vib}(T) = \sum_{i=1}^{3N} \frac{h\omega_i}{2} + kT \sum_{i=1}^{3N} \ln[1 - \exp(-h\omega_i/kT)], \quad (3)$$

where $h\omega_i$ is the DFT-obtained vibrational energy of normal modes, $h$ is Planck's constant, $k$ is the Boltzmann's constant, and $3N$ is the total number of vibrational modes.

In Eq. (1), the $\mu_H(T,P)$ is the H chemical potential related to both temperature $T$ and pressure $P$, and it is often given as [43–45].

$$\mu_H(T,P) = \mu_H(T = 0K) + \mu_H(T \neq 0K, P), \quad (4)$$

where $\mu_H(T = 0K)$ is half of an $H_2$ molecule energy at $T = 0$ K. An $H_2$ molecule energy can be obtained by calculating an $H_2$ molecule putted into a cubic vacuum box with 14.25 Å sides and simultaneously carrying out a zero-point energy (ZPE) correction at $T = 0$ K. According to the present calculation, the energies of an $H_2$ molecule without and with ZPE-correction are −6.76 eV and −6.45 eV, respectively. Therefore, the $\mu_H(T = 0K)$ without and with ZPE-correction are −3.38 eV and −3.255 eV, respectively. As to the $\mu_H(T \neq 0K, P)$, it is dependent on the temperature and $H_2$ gas pressure. In order to effectively compare to experiments, here we will directly use the temperature-dependent $\mu_H(T \neq 0, P_{1atm})$ at one atmosphere pressure, which is written as $\mu_H(T \neq 0, P_{1atm}) = -1.75kT \ln(T/7.55)$ given by Sugimoto et al. [21] and Ji et al. [46]. So, according to Eq. (4), the total H chemical potential with the temperature is given as $\mu_H(T, P_{1atm}) = -1.75kT\ln(T/7.55) - 3.225$ eV.

To obtain the dissolving concentration of H in the interstitial position, we assume that the interstitial H atoms are in the dilute limit in bcc-Fe. According to the H dissolution energy, the H dissolving concentration with the increasing temperature can be given as

$$C_H = \frac{N_{int}}{N} \exp\left(-G_H^d/kT\right), \quad (5)$$

where $N_{int}$ is the number of the tetrahedral interstitial positions, $N$ is the number of Fe atoms. From the present calculations, H is preferable to occupy the tetrahedral interstitial position in bcc-Fe, while Fe belongs to bcc lattice structure, therefore in one cubic cell there are *twelve* tetrahedral interstitial positions and *two* Fe atoms, respectively, then $N_{int}/N$ in the whole bcc-Fe system is equal to *six*.

### *Calculations of H diffusion in bcc-Fe*

According to Arrhenius diffusion theory, the diffusivity of an H atom hopping between two interstitial sites in metal [47] is given by

$$D = D_0 \exp(-G_H^a/kT), \quad (6)$$

where $D_0$ is diffusion pre-exponential factor, $G_H^a$ is the activation energy and it is the difference between the energies of H at the transition state ($G_H^{ts}$) and the initial state ($G_H^{is}$), i.e.,

$$G_H^a = G_H^{ts} - G_H^{is}. \quad (7)$$

Wert and Zener' theory [48] presents that $D_0$ is defined as $\frac{n}{6}(\lambda)^2\sqrt{\frac{2G_H^a}{m\lambda^2}}$ for H atom along the corresponding diffusion route in cubic metal, and here $n$, $\lambda$ and $m$ are the number of the nearest neighbor interstitial lattice site, the jumping length and the mass of H atom, respectively.

The transition state theory [49,50] states that the diffusivity is also written as

$$D = \frac{n}{6}(\lambda)^2\frac{kT}{h}\frac{Z_H^{ts}}{Z_H^{is}}\exp(-G_H^a/kT), \quad (8)$$

where $Z_H^{ts}$ and $Z_H^{is}$ are the total partition functions of the transition state and the initial state, respectively. Also, this formula can be solved for the diffusivity employing either classical or quantum mechanical solution for the vibration partition function. Using the quantum mechanical solution of the vibration partition function, within the harmonic oscillation approximation, the diffusivity is given as

$$D = \frac{n}{6}(\lambda)^2\frac{kT}{h}\frac{\prod_i^{3N-1}\frac{\exp\left(\frac{-h\omega_i^+}{2kT}\right)}{1-\exp\left(\frac{-h\omega_i^+}{kT}\right)}}{\prod_i^{3N}\frac{\exp\left(\frac{-h\omega_i}{2kT}\right)}{1-\exp\left(\frac{-h\omega_i}{kT}\right)}}\exp(-G_H^a/kT), \quad (9)$$

where $\omega_i^+$ and $\omega_i$ are two real normal vibration modes for the transition state and the initial state, respectively, $N$ denotes the number of the vibrating atoms. Note that along the reaction coordinate, the potential energy exhibits a negative curvature, which will yield an imaginary vibration mode ($\omega^*$) at the

transition state (saddle point). Therefore, there is one real normal mode less at the transition state than at the initial state.

The climbing image nudged elastic band (CI-NEB) method [51] was employed to determine minimum energy migration route for the diffusion of H at the interstitial position. Atomic positions are linearly interpolated to set up images along the migrating route connecting the initial and final positions. The artificial springs connect the initial and final positions to construct a band, which is relaxed according to the CI-NEB algorithm to obtain the minimum energy diffusion route and the transition state. The energy difference between the transition state and minimum is energy barrier.

### *Temperature effect description*

In the current study, the temperature effect includes the contributions of two-part, i.e., the thermal expansion of lattice and vibration free energy. The thermal expansion of lattice is related to the temperature. There have been many researches on the thermal expansion behaviors of different structural metals using the experimental and theoretical methods. Lu et al. [52] have recently shown the thermal expansion coefficients of bcc-Fe employing the PARROT module [53] in the Thermo-Calc software package [54], and the calculated results agree fairly with the reported experimental data. Therefore, we will employ the numerical values calculated by Lu et al. [52] to link the temperature and the lattice constant. The temperature-dependent lattice constant ($a_T$) are calculated to use in applying our DFT data by multiplying the ratio $a'_T/a'_0$ proposed by Lu et al. [52] with the current optimized lattice constant at $T = 0$ K ($a_0$), i.e., $a_T = a_0 \cdot (a'_T/a'_0)$. Thus, each $E_{a_T}$ will be obtained from first-principles calculations as the ground-state energy. According to Eq. (3), $F_{vib}(T)$ is related to the vibration modes ($\omega_i$) of the system at a given temperature. The vibration modes and $a_T$ are one-to-one relationship so that the vibration modes of the thermal expansion system will be recalculated for a given $a_T$. After obtaining the $E_{a_T}$ and $F_{vib}(T)$, the dissolution energy and diffusion activation energy of H in bcc-Fe for each given temperature can be calculated by substituting the corresponding "$G(T,P) = E_{a_T} + F_{vib}(T) - TS^{conf}$" into Eqs. (1) and (7). Finally, we can gain how the dissolution energy and diffusion activation energy of H in bcc-Fe alter with the increasing temperature.

## Results and discussion

### *Temperature-dependent lattice constant of bcc-Fe*

We first establish the temperature-dependent lattice constant of bcc-Fe so as to further investigate the effect of thermal expansion on H dissolution and diffusion in bcc-Fe. Lu et al. [52] have given the molar volume of bcc-Fe with the increasing temperature, which is expressed as

$$V_T = V_0 \exp(3.42756 \times 10^{-5}T + 8.14005 \times 10^{-9}T^2 + 0.291672T^{-1}), \quad (10)$$

where $V_T$ and $V_0$ are the molar volumes at the temperature $T$ and 0 K, respectively. Considering the ratio ($a_T/a_0$) of lattice constant, Eq. (10) will further written as

$$a_T/a_0 = \sqrt[3]{\exp(3.42756 \times 10^{-5}T + 8.14005 \times 10^{-9}T^2 + 0.291672T^{-1})}. \quad (11)$$

Using Eq. (11), the temperature-dependent lattice constant of bcc-Fe has been calculated, as listed in Table 2. It can be clearly seen that the lattice constant of bcc-Fe increases significantly with the increase of temperature, which accords with the actual physical rule. For instance, the lattice expansion is close to 1.27% when the temperature increases to 900 K.

### *Dissolution of H in interstitial lattice in bcc-Fe*

*Dissolution energy of H in interstitial lattice at ground state*

In order to compare with the H dissolution behavior at finite temperature, we first simulate the H dissolution property at $T = 0$ K in bcc-Fe. Similar to other studies [10,11,17,26] previously, we take into account two more possible interstitial positions, i.e., tetrahedral interstitial position (TIP) and octahedral interstitial position (OIP). As seen from Table 3, an H atom is energetically preferable to stay at the TIP rather than the OIP. The specific values show that our calculated dissolution energy (0.31 eV) of H at the TIP is in good agreement with the experimental data of 0.29–0.32 eV [7,20,38] and the theoretical results of 0.32 eV [9] and 0.30 eV [10]. However, we note that our predicted result of 0.31 eV is larger by 0.08 eV than 0.23 eV given by Hayward et al. [17]. The small difference might be attributed to the use of different computational codes, i.e., the SIESTA code was employed in Ref. [17] while VASP code is used in this work. For H at the OIP, our result of 0.35 eV with ZPE-correction is larger than 0.26 eV provided by Hayward et al. [17] however smaller than 0.42 eV without ZPE-correction given by Jiang et al. [10]. If Jiang et al. carried out the ZPE-correction, the dissolution energy of H at the OIP will be reduced by 0.035–0.04 eV. In other words, their dissolution energy of H at the OIP will be further decreased to 0.38 eV, well agreeing with our predicted value of 0.35 eV using the same VASP computational code. As to the ZPEs of H at the TIP and OIP, our results are in fair agreement with previous theoretical studies [10,17,26], as listed in Table 3.

**Table 2 – The ratio ($a_T/a_0$) of lattice constant, the lattice constant ($a_T$) and the corresponding lattice expansion strain (%) of bcc-Fe with the increasing temperature.**

| Temperature (K) | $a_T/a_0$ | $a_T$ (Å) | Strain (%) |
|---|---|---|---|
| 0 | 1.0000 | 2.8517 | 0 |
| 300 | 1.0040 | 2.8631 | 0.40 |
| 400 | 1.0053 | 2.8667 | 0.53 |
| 500 | 1.0066 | 2.8705 | 0.66 |
| 600 | 1.0080 | 2.8746 | 0.80 |
| 700 | 1.0095 | 2.8788 | 0.95 |
| 800 | 1.0111 | 2.8832 | 1.11 |
| 900 | 1.0127 | 2.8878 | 1.27 |
| 1000 | 1.0143 | 2.8926 | 1.43 |

**Table 3 – The dissolution energies ($G^d_H$) and ZPE of H at the TIP and OIP as in bcc-Fe at $T = 0$ K including the current calculations and other results of calculations and experiments. $\Delta G^d_{H(OIP-TIP)}$ is the dissolution energy difference of H in the OIP and TIP. All energies are in eV.**

| Property | Other simulations | This work | Expt. |
|---|---|---|---|
| $G^d_{H(TIP)}$ | 0.32[a], 0.30[b], 0.23[c] | 0.31 | 0.29[e], 0.296[f], 0.32[g] |
| $G^d_{H(OIP)}$ | 0.42[b], 0.26[c] | 0.35 | |
| $\Delta G^d_{H(OIP-TIP)}$ | 0.12[b], 0.035[c] | 0.04 | |
| ZPE of $H_{TIP}$ | 0.234[b], 0.24[c], 0.26[d] | 0.25 | |
| ZPE of $H_{OIP}$ | 0.12[c] | 0.13 | |

[a] Ref. [9], GGA with STATE code.
[b] Ref. [10], GGA with VASP code.
[c] Ref. [17], GGA with SIESTA code.
[d] Ref. [26], GGA.
[e] Ref. [38].
[f] Ref. [7].
[g] Ref. [20].

*Dissolution of H in interstitial lattice referring to the temperature-dependent H chemical potential*

Employing Eq. (1), the dissolution energy of H in the TIP and OIP with the alteration of temperature has been calculated in bcc-Fe, as seen from Fig. 1 (a). It is important to see that the H dissolution energy in both interstitial sites increases with the increasing temperature, demonstrating that the needed energy of H dissolving in perfect bcc-Fe will increase with the increasing temperature. In other words, the dissolution of H becomes more and more difficult with the increasing temperature. In terms of the thermodynamic property of impurity dissolving in metal, the H dissolution energy is much larger, the location of H occupying is much more unstable. Therefore, the two interstitial positions for H in bcc-Fe become more and more unstable with the increasing temperature. Furthermore, one notes that the dissolution energy difference between H at two interstitial positions is getting bigger and bigger with the increasing temperature, i.e., the H dissolution energy increases slightly slower with the increasing temperature in the TIP than in the OIP, as shown in Fig. 1 (a). This implies that the TIP for H is slightly more stable than the OIP in bcc-Fe with the temperature.

In order to understand specifically the effect of temperature on the H dissolution energy in bcc-Fe, we decompose the total dissolution energy into two-part energies, i.e., the thermal expansion contribution and phonon vibration contribution. The thermal expansion contribution is the so-called static energy from the DFT calculation for each strained lattice constant $a_T$ at the corresponding temperature, then the H dissolution energy $G^d_{H(strain)}(T = 0K)$ can be given as

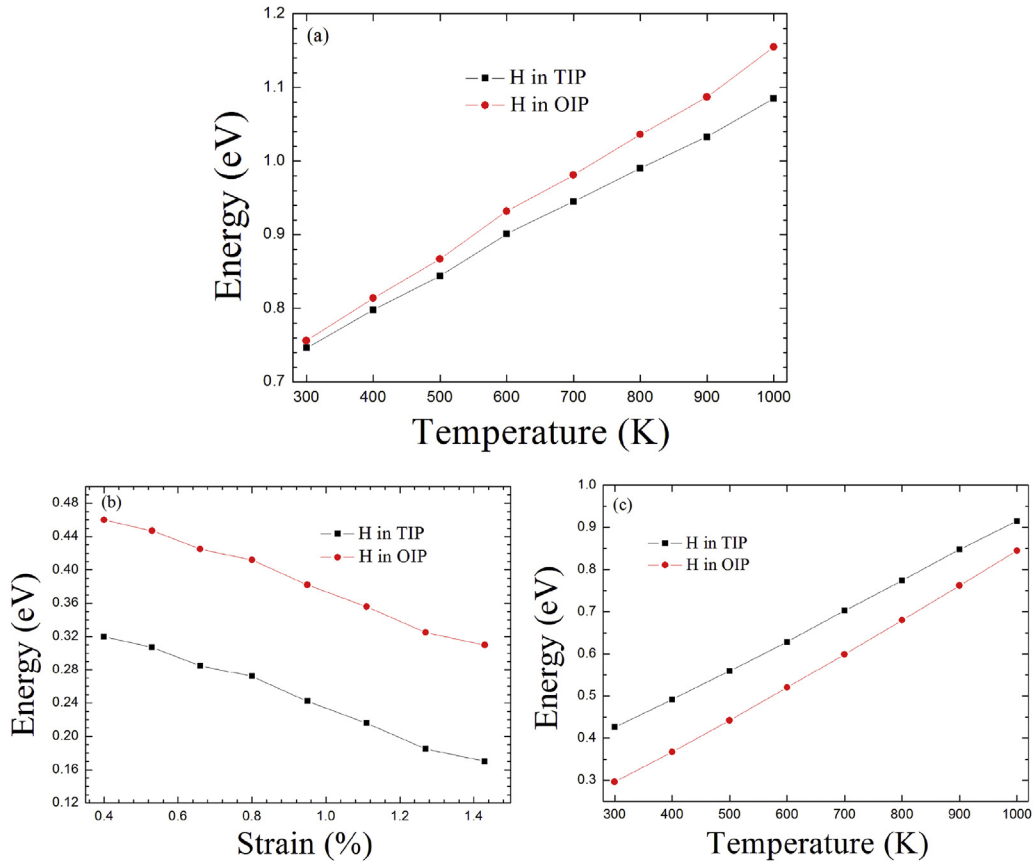


**Fig. 1 – The dissolution energies of H at the TIP and OIP with the increasing temperature in bcc-Fe. (a) The total dissolution energy. (b) The static dissolution energy in reference to the H chemical potential $\mu_H(T = 0K)$, which are relevant with lattice expansion caused by temperature increase. (c) Phonon vibration dissolution energy referring to the temperature-dependent H chemical potential $\mu_H(T \neq 0K)$.**

$$G^{d}_{H(strain)}(T=0K) = E_{a_T(H-Fe)} - E_{a_T(Fe)} - \mu_H(T=0K), \quad (12)$$

where $E_{a_T(H-Fe)}$ and $E_{a_T(Fe)}$, respectively, represent the DFT static energies of H-Fe and perfect Fe system for each strained lattice constant $a_T$ at the corresponding temperature. While the H dissolution energy of phonon vibration contribution can be expressed as

$$G^{d}_{H(vibration)}(T) = F^{vib}_{a_T(H-Fe)}(T) - F^{vib}_{a_T(Fe)}(T) - \mu_H(T\neq 0K, P_{1atm}), \quad (13)$$

where$F^{vib}_{a_T(H-Fe)}(T)$ and $F^{vib}_{a_T(Fe)}(T)$, respectively, are phonon vibration energies of H-Fe and perfect Fe systems for each strained lattice constant $a_T$ at temperature $T$. As a matter of fact, the H chemical potential has been divided into two parts, i.e.,$\mu_H(T=0K)$ and $\mu_H(T\neq 0K, P_{1atm})$.

Fig. 1(b) gives the altering curve of the H dissolution energy from the thermal expansion contribution with the increase of temperature in bcc-Fe. It can be seen that the H dissolution energy decreases in a close-linear form with the increasing strain (temperature), indicating that the thermal expansion (here the thermal expansion corresponds to the isotropic tensile strain) can reduce the H dissolution energy in bcc-Fe, similar to the dissolution behavior of impurity carbon in metal Pd [55]. The reduced energies from 300 to 1000 K are 0.15 and 0.16 eV for H in the TIP and OIP, respectively. We also find that the dissolution energy difference of H in the OIP and TIP is invariably close to 0.14 eV. This means that the thermal expansion can neither alter the H relative stability nor change the dissolution energy difference between H in two interstitial positions. On the whole, one sees from Fig. 1(b) that there are two main characteristics on the expansion-induced H dissolution energy in bcc-Fe: one is the H dissolution energy decreasing "monotonically" with the increasing isotropic tensile strain; the other is the H dissolution energy in a close-linear form depending negatively on the temperature. The two characteristics could be understood as follows.

The first characteristic can refer to the homogeneous electron gas model in the earlier study [56]. According to this model, the H dissolution energy reduces monotonically with decreasing electron density until reaching the minimum at an optimal electron density, but which is not completely suitable for the metallic environment. More recently, tungsten as an example, we have given an optimal electron density mechanism [57] in a metallic environment for H dissolution. In a metallic environment, the H dissolution energy also reduces with the decreasing electron density. Vacancy internal surface can be found to provide the optimal electron density region for H binding [57]. The optimal electron density values are ~0.11 electron/Å$^3$ in tungsten in our previous study [57] and ~0.12 electron/Å$^3$ in bcc-Fe in the current calculation, respectively. Similarly, this mechanism can indicate that at a given interstitial position in tungsten or bcc-Fe, the lower electron density, the lower H dissolution energy. Such a mechanism is found to be generally applicable for H in most transition metals and metal-alloys [57]. Back to the current H-Fe system, taking the TIP as an example, the electron density of TIP without tensile strain are calculated to be ~0.25 electron/Å$^3$ in bcc-Fe. With the increase of isotropic tensile strain, the electron density of the TIP decreases gradually, as shown in Fig. 2.

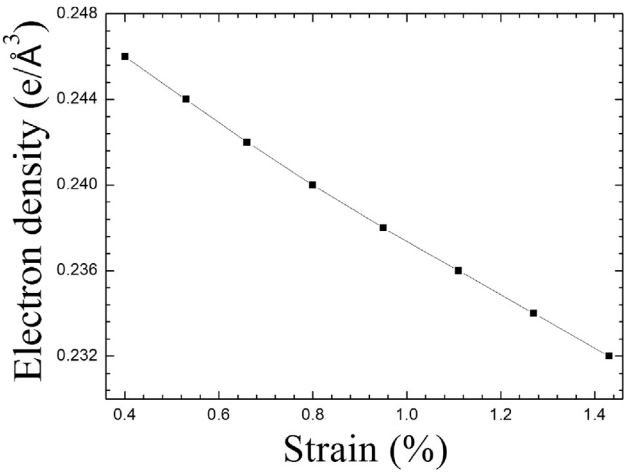


**Fig. 2 – The electron density of the TIP with the increase of isotropic strain in bcc-Fe. Note that the strain and temperature are one-to-one correspondence.**

When the tensile strain reaches 0.80% (corresponds to $T = 600$ K), the electron density reduces to ~0.241 electron/Å$^3$. With the further increase of isotropic tensile strain, the electron density further decreases. As the strain expands to 1.43% (corresponds to $T = 1000$ K), the electron density will decrease to ~0.23 electron/Å$^3$. Although the reduction of the electron density is not very large from 300 to 1000 K, the electron density of ~0.232 electron/Å$^3$ at $T = 1000$ K is getting closer to the optimal electron density of ~0.12 electron/Å$^3$ than that at $T = 300$ K (~0.246 electron/Å$^3$) in bcc-Fe. Therefore, the gradually reduced electron density results in the gradually decreased dissolution energy of H in the TIP in bcc Fe. The similar analysis can be also applicable for H in the OIP in bcc-Fe.

The second characteristic is that the H dissolution energy in a close-linear form depends negatively on the temperature, which can be explained by the linear elasticity theory [58]. The linear elasticity theory states that the H dissolution energy in metals under thermal expansion (tensile strain) is given as $G^{d}_{\varepsilon} = G^{d}_{\varepsilon=0} + (\sigma_{[100]}\varepsilon_{[100]} + \sigma_{[010]}\varepsilon_{[010]} + \sigma_{[001]}\varepsilon_{[001]})V_{\varepsilon=0}$, where $G^{f}_{\varepsilon=0}$ is the H dissolution energy without expansion, $\sigma_{[m\ ln]}$ is the thermal expansion-induced lattice stress at each crystal-direction in the equilibrium system, $\varepsilon$ is the strain, and $V_{\varepsilon=0}$ is the volume of the metal system (here, the system is bcc-Fe supercell) without expansion at equilibrium state. The current thermal expansion is isotropic strain because Fe belongs to the cubic crystal system, i.e., $\varepsilon_{[100]} = \varepsilon_{[010]} = \varepsilon_{[001]}$, while $\sigma_{[100]} + \sigma_{[010]} + \sigma_{[001]}$ should be approximately equal to $3\bar{\sigma}$ ($\bar{\sigma}$ is the average stress and it is given as $\bar{\sigma} = \frac{1}{3}(\sigma_{[100]} + \sigma_{[010]} + \sigma_{[001]})$ ), therefore the H dissolution energy can be further given as $G^{f}_{\varepsilon} = G^{f}_{\varepsilon=0} + 3\bar{\sigma}V_{\varepsilon=0}\varepsilon$. We can clearly see that there is a linear dependence of H dissolution energy $G^{f}_{\varepsilon}$ on strain $\varepsilon$ with a slope $3\bar{\sigma}V_{\varepsilon=0}$. Due to that the average stress $\bar{\sigma}$ is compressive (negative by convention when the lattice is stretched in the current calculations), the H dissolution energy negatively alters in a close-linear form with the increasing tensile strain in both TIP and OIP.

As shown in Fig. 1(c), the H dissolution energy from phonon vibration contribution also presents a temperature-dependent property in bcc-Fe. Although the phonon vibration energy is related to the term of the ~exp($-h\omega_i/kT$) form given in Eq. (3), the H dissolution energy in both TIP and OIP changes positively in a quasi-linear form with the increasing temperature. In other words, the H dissolution energy from phonon vibration contribution exhibits an opposite changing trend, compared with the lattice thermal expansion contribution. According to Eq. (13), the energy reference point is not the static H chemical potential $\mu_H(T=0K)$, but the temperature-dependent H chemical potential $\mu_H(T\neq 0K, P_{1atm})$. We might understand the H dissolution energy increasing linearly with the temperature as the following. According to the current calculation, the absolute value of phonon vibration energy is much lower than that of H chemical potential $\mu_H(T\neq 0K, P_{1atm})$ at each given temperature. For instance, at $T=800$ and 1000 K, phonon vibration energies of H at the TIP are only 0.21 and 0.18 eV, respectively, while the $\mu_H(T=500K, P_{1atm})$ and $\mu_H(T=900K, P_{1atm})$ are −0.56 eV and −0.735 eV, respectively. Therefore, the temperature-dependent H chemical potential in Eq. (13) dominates mainly the temperature-dependent H dissolution energy, and as a result of the energy–temperature curve exhibiting a quasi-linear positively altering trend (Fig. 1(c)).

*Dissolution of H in interstitial lattice referring to the static H chemical potential*

The above results demonstrate that the total dissolution energy (two parts: the lattice thermal expansion contribution and phonon vibration contribution) of H in both TIP and OIP increases with the increasing temperature at one atmosphere pressure in bcc-Fe. However, if we only use the static H chemical potential $\mu_H(T=0K)$ as the reference energy, there will be an opposite conclusion on the H dissolution energy with the increasing temperature in bcc-Fe, i.e., the H dissolution energy decreases with the increasing temperature, as shown in Fig. 3(a). Similar to the above analysis method, the H dissolution energy can be also decomposed into two part contributions, i.e., thermal expansion ($G^d_{H(strain)}$) and phonon vibration ($G^d_{H(vibration)}$), which are, respectively, given as

$$G^d_{H(strain)} = E_{a_T(H-Fe)} - E_{a_T(Fe)} - \mu_H(T=0K), \tag{14}$$

and

$$G^d_{H(vibration)} = F^{vib}_{a_T(H-Fe)}(T) - F^{vib}_{a_T(Fe)}(T). \tag{15}$$

Actually, Eq. (14) is the same as Eq. (12) given above, while Eq. (15) has gotten rid of the temperature-relevant $\mu_H(T\neq 0K, P_{1atm})$ compared with Eq. (13).

Based on Eqs. (14) and (15), we recalculate the H dissolution energy in both TIP and OIP in bcc-Fe. Fig. 3(b) gives the dissolution energy of interstitial H as a function of temperature in reference to the static H chemical potential $\mu_H(T=0K)$ in bcc-Fe. As expected, the H dissolution energy in both TIP and OIP from thermal expansion contribution displays the same changing trend as the above analysis, due to that Eq. (14) is equal to Eq. (12). We further analyze the H dissolution energy from phonon vibration energy contribution, i.e., $F^{vib}_{a_T(H-Fe)}(T) - F^{vib}_{a_T(Fe)}(T)$ defined by Eq. (15). As clearly seen from Fig. 3(c), the H vibration dissolution energy in bcc-Fe decreases exponentially in both interstitial positions with the increasing temperature. This should be attributed to that the vibrational Helmholtz free energy exhibits the exponential term (~exp($-h\omega_i/kT$)). At the same time, the H vibration dissolution energy decays much faster with the increase of temperature in the TIP than in the OIP. When the temperature increases from 300 to 1000 K, the decreased vibration dissolution energy in the TIP and OIP are 0.08 and 0.02 eV, respectively. This is originated from that the TIP and OIP exhibit the different numbers of vibration modes. According to the above analysis, the TIP for H is the most stable position in bcc-Fe. Correspondingly, there are three vibration modes of H at the ground state with two degenerate frequencies and one smaller frequency. Whereas, the OIP for H is a transition state, which is just the saddle point for H migrating from one TIP to first nearest neighbor TIP (see 3.3 section), and thus there are only one real normal modes and two imaginary mode in reference to the negative curvature of the saddle point. The fewer vibration modes of in the OIP leads to that the H vibration dissolution energy reduces more slowly with the increase of temperature in the OIP than in the TIP.

*Dissolving concentration of H in bcc-Fe*

We present two different ways above to obtain the interstitial H dissolution energy in bcc-Fe, resulting in different changing trend of the total H dissolution energy, i.e., the H dissolution energy either "increases" or "decreases" with the increasing temperature. Two different conclusions are attributed to two different choices of H chemical potential: one through referring to the static H chemical potential $\mu_H(T=0K)$ and the other through referring to a temperature-dependent H chemical potential $\mu_H(T\neq 0K, P_{1atm})$. If we choose $\mu_H(T=0K)$ as the energy reference point, the H dissolution energy decays with the increase of temperature. If the energy reference point is chosen as $\mu_H(T\neq 0K, P_{1atm})$, the H dissolution energy increases significantly with the increasing temperature. Objectively speaking, the temperature-dependent H dissolution energy in reference to the temperature-dependent H chemical potential should be more in line with the actual case. Physically, it is well known that the total energy of the whole material system will increase with the increasing temperature because the electrons will produce the strong motion with the increasing temperature [59,60]. If impurity H wants to live in such a higher energy environment, it will have to get a much higher energy from the external environment. This will directly result in an increase of the H dissolution energy. Recently, the theoretical study has showed that Gibbs free energy including the DFT static energy and vibrational Helmholtz free energy at finite-temperature can effectively predict the H adsorption energy in reference to the "temperature-dependent H chemical potential $\mu_H(T,P)$" in metal-porphyrin-incorporated graphene [61].

In view of the above discussion, in the following concentration calculation, we only take into account the temperature-dependent H dissolution energy. Fig. 4 plots the dissolving concentration of H as a function of the reciprocal of temperature from 300 to 1000 K. Despite the H dissolution energy is temperature-dependent, it can be clearly seen from Fig. 4 that the calculated H concentration can still obey the

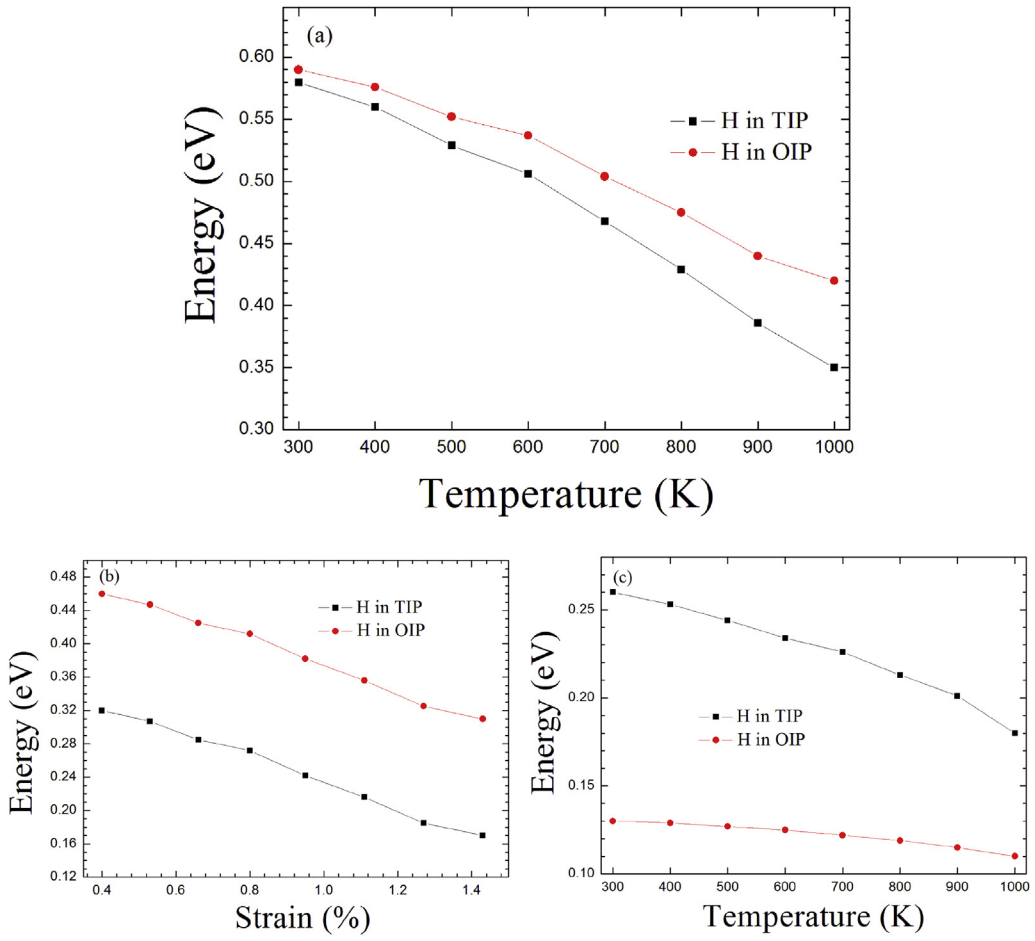


**Fig. 3 – The dissolution energies of H in the TIP and OIP with the increasing temperature in bcc-Fe. (a) The total dissolution energies. (b) The dissolution energies from thermal expansion (strain) contribution in reference to a static H chemical potential $\mu_H(T = 0K)$. (c) The dissolution energies from phonon vibration contribution without any reference points.**

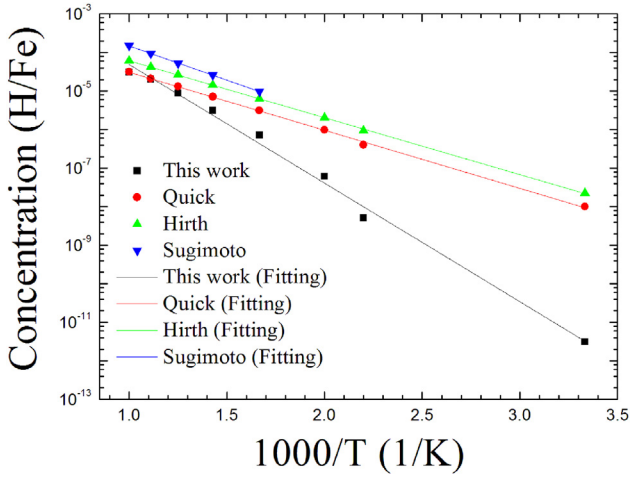


**Fig. 4 – The dissolving concentration of H as a function of the reciprocal of temperature at one atmosphere pressure in bcc Fe. Experimental data are also given from Quick [20], Hirth [7], and Sugimoto [21] in bcc-Fe.**

Arrhenius-kind changing curve with the temperature so that we can give the fitted Arrhenius dissolution equation with the form $S = S_0\exp(-G_0/kT)$, where $S_0$ and $G_0$ denote the dissolution pre-factor and activation energy, respectively. The fitted pre-factor and activation energy are $1.17 \times 10^{-2}$ and 0.49 eV, respectively. Correspondingly, the fitted Arrhenius dissolution equation is given as $S(H/Fe) = 1.17 \times 10^{-2}\exp(-0.49\,eV/kT)$. Within the error range, the fitted Arrhenius dissolution equation is close to the experimental results provided by et al. [20] $S(H/Fe) = (0.28–11.91) \times 10^{-3}\exp[-(0.293 \pm 0.028)eV/kT]$ and Sugimoto et al. [21] $S(H/Fe) = 0.82 \times 10^{-2}\exp(-0.35\,eV/kT)$, respectively. The agreement with experiment is an important criterion to validate the current theoretical calculations. We note from Fig. 4 that at low temperature regime from 300 to 700 K, the calculated H concentration exhibits a significant deviation from the experimental data. This suggests that the H dissolution concentration is strongly influenced by the defect-capturing effect at low temperature. It is well known that defects such as vacancies and dislocations must appear in material. In the present study, we do not take into account these defects in bcc-Fe. Both vacancies and stacking faults have been demonstrated to serve as the capturing center of H atoms in many transition metals. Moreover, these captured H

atoms can significantly weaken and break the intrinsic metallic bonds in the vicinity of vacancy and stacking fault, which in turn leads to accumulation of more H atoms in the vicinity of vacancy and stacking fault. As a result, comparing with the current results calculated in defect-free bcc-Fe, the higher H concentration obtained from experiments in actual bcc-Fe is reasonable at the low temperature range. However, with the temperature above 700 K, our calculated H concentration is in fair agreement with the experimental data, as shown in Fig. 4. For instance, the H concentrations in bcc-Fe are calculated to be $0.88 \times 10^{-5}$(H/Fe) at $T = 800$ K and $3.06 \times 10^{-5}$(H/Fe) $T = 1000$ K, which are in quantitative agreement with experimental data [20] of $1.32 \times 10^{-5}$(H/Fe) at $T = 800$ K and $3.14 \times 10^{-5}$(H/Fe) $T = 1000$ K, respectively. On the other hand, the high-temperature consistency and the low-temperature deviation can also suggests that the temperature effect must be taken into account to accurately interpret experimental data of H dissolving in bcc-Fe as well as other metals.

### *Diffusion behaviors of H isotope at finite temperature*

Now, we analyze the diffusion properties of H at finite temperature in bcc-Fe. The above thermodynamic results demonstrate that the TIP for H is the most stable location in bcc-Fe. Therefore, we allow the H atom to migrate from one TIP to another neighbor one, and thus there are two different migrating routes, as plotted in Fig. 5(a). For the first diffusion route, as seen from Fig. 5(b), H atom migrates from one TIP to its first nearestneighbor (1NN) TIP via a mediate transition state, and then we call this route as T→T route. For the second diffusion route, H atom moves from one TIP to its 2NN TIP, crossing an mediate OIP (Fig. 1(b)), correspondingly we name this path as T→O→T route. As to the T→T route, the transition state of H is situated in a position which is off mediate position between two 1NN TIPs near an OIP. For the T→O→T route, the OIP is just the saddle point (transition state), and thus the H diffusion activation energy is the energy difference between H at the TIP and OIP.

Employing Eq. (7), the H diffusion activation energy as a function of temperature in bcc-Fe have been obtained, as given in Fig. 6(a). It is important to note that the energy barrier

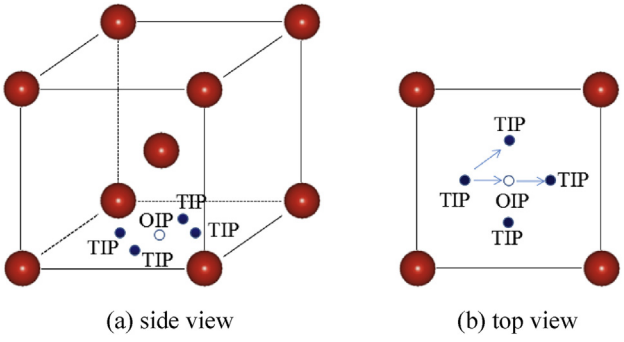


**Fig. 5 – The TIP (blue/solid point) and OIP (white/open point) in bcc-Fe lattice. The larger spheres represent Fe atoms. (For interpretation of the references to colour in this figure legend, the reader is referred to the web version of this article.)**

in both diffusion routes increases with the increase of temperature, and the value changes from 0.049/0.047 eV to 0.089/0.087 eV for T→T/T→O→T route with the temperature altering from 300 to 1000 K. This implies that the needed energy to overcome the transition state for H migrating along two diffusion routes will increase with the increasing temperature in bcc-Fe. Also, we can see from Fig. 6(a) that the T→O→T route displays a viable transition pathway for H with the slightly lower barrier in comparison with T→T route at each given temperature point. It seems to be in contradiction with the conclusion of the static state condition ($T = 0$ K) obtained by previously most studies [10,11,26], in which the T→T route was demonstrated to be more preferable than the T→O→T route. However, our calculation is in agreement with recent theoretical result by Hayward et al. [17] who give that the T→O→T route is energetically preferable to the T→T route with the ZPE correction. Taking into account the precision of our calculations, both energy barriers of H along these two diffusion routes are essentially equivalent and quite small. During the optimization, All the energy were converged to within less than $10^{-4}$ eV/atom, giving the energy barriers of 0.049–0.089 eV and 0.047–0.087 eV for T→T and T→O→T routes, respectively. On the other hand, we believe that both diffusion routes should be potentially possible, since the small energy difference between two paths appears at any given temperature. On the whole, our predicted H diffusion activation energy with the temperature from 300 to 1000 K can well fall into the experimental range of 0.03–0.14 eV [7,20,25].

To gain some physical insights on H diffusion activation energy increasing with the temperature, similar to the above analysis, we also decompose the total activation energy into two parts, i.e., the thermal expansion contribution and phonon vibration contribution. Based on Eq. (7), the energy barrier from thermal expansion contribution can be given as $G^{a}_{H(a_T)} = G^{ts}_{H(a_T)} - G^{is}_{H(a_T)}$, while the energy barrier from phonon vibration contribution is expressed as $G^{a}_{H(vibration)} = G^{ts}_{H(vibration)} - G^{is}_{H(vibration)}$. Differing from the above H dissolution energy, the H diffusion activation energy is not related to the H chemical potential, due to that it is the energy difference between H at two positions. As shown in Fig. 6(b), with the temperature increasing from 300 to 1000 K, the H energy barriers from thermal expansion contribution alter from 0.089 to 0.079 eV for the T→T route and from 0.147 to 0.137 eV for the T→O→T route, respectively. In other words, the diffusion activation energy of H along both migrating routes slightly decreases with the increasing temperature. Such phenomenon should be attributed to that the lattice expansion can result in the increase of lattice constant so as to enlarge the effective moving space of H atom and reduce the H diffusion difficulty. At the same time, we might believe that the H activation energy from thermal expansion contribution slightly depends on the temperature, due to that the reduced value is much small and only 0.01 eV for both diffusion routes. Whereas, according to Fig. 6(c), the H energy barriers from phonon vibration contribution for both diffusion routes are significantly dependent on the temperature and increase with the increasing temperature, and the energies range from −0.04 eV to 0.01 eV and −0.10 eV to −0.05 eV when the temperature increases from 300 to 1000 K for T→T and T→O→T routes, respectively. This means that phonon

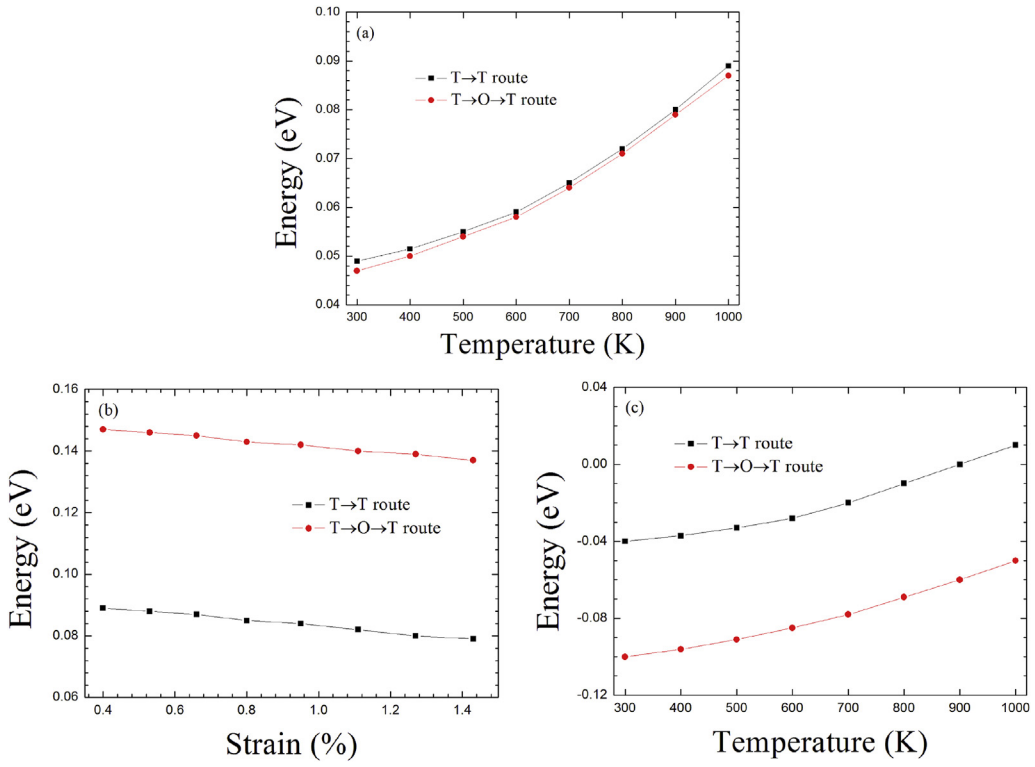


**Fig. 6 – Along the T→T and T→O→T routes, the H diffusion activation energy as a function of temperature or strain in bcc-Fe. (a) The total diffusion activation energies. (b) The diffusion activation energies from the lattice expansion contribution. (c) The diffusion activation energies from phonon vibration contribution.**

vibration energy contribution plays a decisive role in the increment of total H activation energy with the increasing temperature.

Employing Eq. (9), we calculated the H diffusivity as a function of the reciprocal of temperature in bcc-Fe, as shown in Fig. 7. Although the diffusion activation energy and pre-factor are related to the temperature, the H diffusivity displays the nearly qusi-Arrhenius curve. As a result, there should be two fitted Arrhenius diffusion equations. The fitted Arrhenius diffusion equations are $D = 5.64 \times 10^{-8}\exp(-0.041/kT)$ $m^2/s$ and $D = 5.56 \times 10^{-8}\exp(-0.039/kT)$ $m^2/s$ for T→T and T→O→T routes, respectively. Experimentally and theoretically, the interstitial H diffusivity in bcc-Fe are also given at the different temperature in Fig. 7. Within the error range, our calculated results at the temperature range from 300 to 1000 K agrees basically with experimental data reported by Hirth [7] and Nagano [24] as well as the theoretical results obtained by Sanchez [19]. Additionally, our predicted results are about one order of magnitude higher than the experimental values given by Kiuchi et al. [25]. This could be explained that a larger diffusion activation energy of ~0.07 eV is used in their diffusion equation.

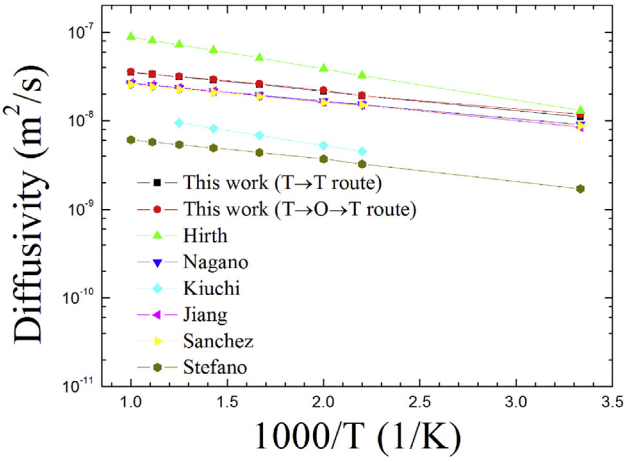


**Fig. 7 – The diffusivity (*D*) of H as a function of reciprocal of temperature in bcc Fe. Experimental results are also given from Hirth [7], Nagano [24], Kiuchi [25]. Other simulated data are obtained from Jiang [10], Sanchez [11] and Stefano [26].**

For completeness, we also give the diffusivity of H isotopes including deuterium and tritium in bcc-Fe. Wert and Zener' theory [48] hints the diffusion pre-factor is given as $D_0 = \frac{n}{6}(\lambda)^2\sqrt{\frac{2G_H^a}{m\lambda^2}}$, meaning that the pre-factors of H, deuterium, and tritium exhibit the following mass ratio relation $1 : \frac{1}{\sqrt{2}} : \frac{1}{\sqrt{3}}$. Thus, the diffusivities of deuterium and tritium can be further calculated in bcc-Fe. As seen from Fig. 8, the diffusivity of deuterium or tritium is clearly lower than that of H. This should be the embodiment of the larger atomic masses of deuterium and tritium.

To our best knowledge, up to now, the pre-factor $D_0$ and activation energy $G_H^a$ are averagely treated as constants with the increasing temperature, and they are almost derived from

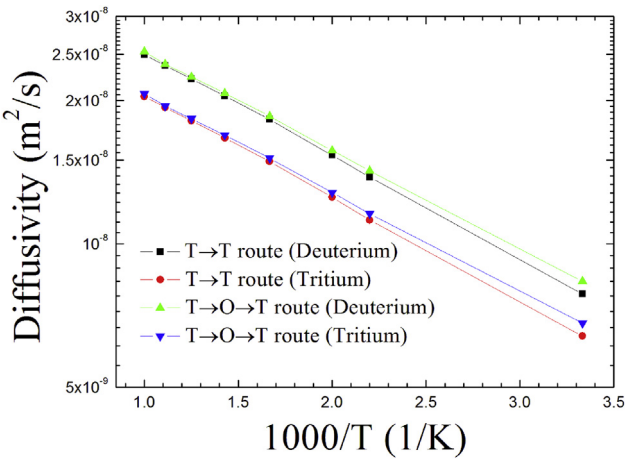


**Fig. 8 – The diffusivity (*D*) of H isotopes including deuterium and tritium as a function of reciprocal of temperature in bcc-Fe.**

the general Arrhenius form $D = D_0\exp(-G_H^a/kT)$. But, this does not comply with the actual situation. In the past, there were many experimental and theoretical investigations indicating that the pre-factor $D_0$ and activation energy $G^a_{impurity}$ of impurity are related to the temperature [55,62,63]. For instance, Yokoyama et al. studied the diffusion properties of impurity carbon in palladium experimentally [64] and found that there exists a lower energy barrier at a lower temperature and a higher energy barrier at a higher temperature. Such incremental behavior of impurity diffusion activation energy with the temperature is again attested by the current interstitial H diffusion in bcc-Fe. Actually, based on the current first-principles total energy and vibrational spectrum calculations combined with transition state theory, we can theoretically predict the temperature-dependent diffusion activation energy and pre-factor of H or other impurity in bcc-Fe (as well as other transition metals). This is because the H diffusion activation energy is the energy difference between H at the transition state and the initial state (see Eq. (7)), while the transition or initial state energy of the H-metal system alters generally with the temperature according to Eqs. (1)–(3). Based on Wert and Zener's theory [48], the pre-factor is defined as $\frac{n}{6}(\lambda)^2\sqrt{\frac{2G_H^a}{m\lambda^2}}$, which obviously depends on the diffusion activation energy $G_H^a$. Thus, the diffusion pre-factor also varies with the temperature.

Referring to the Arrhenius diffusion equation, we have to discuss the interdependent relationship between the thermal activation energy and pre-factor, due to that the diffusion of H in bcc-Fe involves the thermally activated processes. It is well known that the most thermally activated processes obey the empirical Arrhenius equation $R = R_0\exp(-G/kT)$, i.e., the measured or calculated diffusion rate $R$ alters with the temperature $T$, where $G$ and $R_0$ the activation energy and pre-factor, respectively. Large amount of experimental observations [64] and theoretical calculations including previous [55,62,63] and current studies have demonstrated that, with the alteration of activation energy, the pre-factor $R_0$ does not always keep constant but rely exponentially on the activation energy $G$, i.e., $R_0 = R_0'\exp(-G/\phi)$. This can lead to that a plot of the activation energy vs the logarithm of the pre-factor is a straight line that is given as $G = \phi\ \ln R_0 + \varphi$, where both $\phi$ and $\varphi$ are constants [65]. The physical mechanism underlying the relationship between activation energy and pre-factor might be originated from the compensation effect [66]. The compensation effect has been successfully applicable for different physical or physico-chemical processes, e.g., the impurity atom diffusion in single-crystal [67] or poly-crystal [65]. For the current H-Fe system, the increase of the pre-factor can directly compensate the modification of the calculated H diffusivity if the H diffusion activation energy varies with the increasing temperature. In other words, such an interdependent relationship between the pre-factor and activation energy can directly cause that the calculated H diffusivity exhibits the Arrhenius-like curve in bcc-Fe.

## Conclusions

Based on first-principles total energy and vibrational spectrum calculations, we investigate the finite-temperature dissolution and diffusion behaviors of H in the interstitial lattice position in bcc-Fe, because of that the dissolution and diffusion of H in bcc-Fe are fundamental and essential data in the H energy application from nuclear conversion. For the temperature effect, we take into account two parts, i.e., the thermal expansion contribution and phonon vibration contribution. The specific conclusions are as follows.

A single H atom is always favorable to occupy the tetrahedral site rather than the octahedral one over the whole considered temperature range of 300–1000 K, and thus the site occupancy of H in bcc-Fe is independent of the temperature. Whereas, the H dissolution energy in both interstitial sites are not invariably kept as constant but temperature-dependent in bcc-Fe. In both interstitial sites, the H dissolution energy referring to the static H chemical potential decreases with the temperature, while the H dissolution energy referring to the temperature-dependent H chemical potential increases with the temperature. With the increasing temperature from 300 to 1000 K, phonon vibration energy contribution plays a key role in the H dissolution energy, while the thermal expansion energy contribution has little influence on the H dissolution energy. Using the temperature-dependent H dissolution energy, we calculate the dissolving concentration of interstitial H at one atmosphere pressure in bcc-Fe. When the temperature is above 700 K, our calculated H concentration is in fair agreement with the experimental data; while the temperature is below 700 K, the predicted H concentration exhibits a significant deviation from the experimental result. This stems from that we do not take into account defects such as vacancies and dislocations because these defects can effectively capture large amount of H atoms so as to enhance the H dissolution in bcc-Fe.

For the interstitial H diffusion in bcc-Fe, we take into account T→T and T→O→T routes, respectively. The activation energy barrier in both diffusion routes increases significantly with the increasing temperature, and the value alters from 0.049/0.047 eV to 0.089/0.087 eV for T→T/T→O→T route with the temperature from 300 to 1000 K. Both diffusion routes in bcc-Fe should be potentially possible, since the energy

difference between two paths is extremely small at any given temperature. With the increasing temperature from 300 to 1000 K, phonon vibration energy contribution plays a crucial role in H activation energy, while the thermal expansion energy contribution has little influence on the H activation energy. Our calculated H activation energy can well fall into the experimental range of 0.03–0.14 eV. Finally, we predict the H diffusivity, which is in quantitative agreement with the experimental data at temperature range from 300 to 1000 K in bcc-Fe.

## Acknowledgments

This research is supported by the National Magnetic Confinement Fusion Program (Grant Nos. 2013GB109002 and 2015GB109001) and the National Natural Science Foundation of China (NSFC) with Grant No. 11575153.

## REFERENCES

[1] Zieliński A, Sobieszczyk S. Hydrogen-enhanced degradation and oxide effects in zirconium alloys for nuclear applications. Int J Hydrog Energy 2011;36:8619–29.
[2] Germeshuizen LM, Blom PWE. A techno-economic evaluation of the use of hydrogen in a steel production process, utilizing nuclear process heat. Int J Hydrog Energy 2013;38:10671–82.
[3] Joseph-Auguste C, Cheikhravat H, Djebaïli-Chaumeix N, Deri E. On the use of spray systems: an example of R&D work in hydrogen safety for nuclear applications. Int J Hydrog Energy 2009;34:5970–5.
[4] Díaz V, Teliz E, Ruiz F, Martínez PS, Faccio R, Zinola F. Molybdenum effect on the kinetic behavior of a metal hydride electrode. Int J Hydrog Energy 2013;38:12811–6.
[5] Solntceva ES, Taubin ML, Bochkov NA, Solntsev VA, Yaskolko AA. Use of tungsten single crystals to enhance nuclear reactors structural elements properties. Int J Hydrog Energy 2016;41:7206–12.
[6] Momida H, Asari Y, Nakamura Y, Tateyama Y, Ohno T. Hydrogen-enhanced vacancy embrittlement of grain boundaries in iron. Phys Rev B 2013;88:144107.
[7] Hirth JP. Neutron radiography study of hydrogen desorption in technical iron. Metall Trans A 1980;11A:861.
[8] Irigoyen B, Ferullo R, Castellani N, Juan A. The location of a hydrogen atom and hydrogen molecules in BCC Fe: an ASED-MO approach. Model Simul Mater Sci Eng 1995;3:319.
[9] Tateyama Y, Ohno T. Stability and clusterization of hydrogen-vacancy complexes in α-Fe: an ab initio study. Phys Rev B 2003;67:174105.
[10] Jiang DE, Carter EA. Diffusion of interstitial hydrogen into and through bcc Fe from first principles. Phys Rev B 2004;70:64102.
[11] Sanchez J, Fullea J, Andrade C, Andres PL. Hydrogen in α-iron: stress and diffusion. Phys Rev B 2008;78:014113.
[12] Matsumoto R, Inoue Y, Taketomi S, Miyazaki N. Influence of shear strain on the hydrogen trapped in bcc-Fe: a first-principles-based study. Scr Mater 2009;60:555–8.
[13] Counts WA, Wolverton C, Gibala R. First-principles energetics of hydrogen traps in α-Fe: point defects. Acta Mater 2010;58:4730.
[14] Hayward E, Deo C. J Phys Condens Matter 2011;23:425402.
[15] Ohsawa K, Eguchi K, Watanabe H, Yamaguchi M, Yagi M. Configuration and binding energy of multiple hydrogen atoms trapped in monovacancy in bcc transition metals. Phys Rev B 2012;85:094102.
[16] Hayward E, Beeler B, Deo C. Multiple hydrogen trapping at monovacancies. Phil Mag Lett 2012;92:217.
[17] Hayward E, Fu CC. Interplay between hydrogen and vacancies in α-Fe. Phys Rev B 2013;87:174103.
[18] Fukai Y. The metal-hydrogen system. Berlin: Springer; 1993.
[19] Oriani RA. Fundamental aspects of stress corrosion cracking, NACE-1. Houston, TX: NACE; 1969. p. 32–49.
[20] DaSilva JRG, McLellan RB. The solubility of hydrogen in super-pure-iron single crystals. J Less-Common Met 1976;50:1.
[21] Sugimoto H, Fukai Y. Solubility of hydrogen in metals under high hydrogen pressures: thermodynamical calculations. Acta Metall 1992;40:2327.
[22] San-Martin A, Manchester FD. In: Okamoto H, editor. Phase diagrams of binary iron alloys. Materials Park, OH: ASM International; 1993. p. 161.
[23] Völkl J, Alefeld G. In: Alefeld G, Völkl J, editors. Hydrogen in metals I. Berlin: Springer; 1978. p. 321.
[24] Nagano M, Hayashi Y, Ohtani N, Isshiki M, Igaki K. Hydrogen diffusivity in high purity alpha iron. Scr Met 1982;16:973.
[25] Kiuchi K, Mclellan RB. The solubility and diffusivity of hydrogen in well-annealed and deformed iron. Acta Metall 1983;31:961.
[26] Stefano DD, Mrovec M, Elsasser C. First-principles investigation of quantum mechanical effects on the diffusion of hydrogen in iron and nickel. Phys Rev B 2015;92:224301.
[27] Batchelder FW, Raeuchle RF. Re-examination of the symmetries of iron and nickel by the powder method. Acta Cryst 1954;7:464.
[28] Li WY, Zhang Y, Zhou HB, Jin S, Lu GH. Stress effects on stability and diffusion of H in W: a first-principles study. Nucl Instrum Methods Phys Res Sect B 2011;269:1731.
[29] Kresse G, Hafner J. Ab initio molecular dynamics for liquid metals. Phys Rev B 1993;47:558.
[30] Kresse G, Furthmüller J. Efficient iterative schemes for ab initio total-energy calculations using a plane-wave basis set. Phys Rev B 1996;54:11169.
[31] Perdew JP, Chevary JA, Vosko SH, Jackson KA, Pederson MR, Singh DJ, et al. Atoms, molecules, solids, and surfaces: applications of the generalized gradient approximation for exchange and correlation. Phys Rev B 1992;46:6671.
[32] Perdew JP, Burke K, Ernzerhof M. Perdew, Burke, and Ernzerhof reply. Phys Rev Lett 1998;80:891.
[33] Perdew JP, Burke K, Ernzerhof M. Generalized gradient approximation made simple. Phys Rev Lett 1996;77:3865.
[34] Blochl PE. Projector augmented-wave method. Phys Rev B 1994;50:17953.
[35] Kresse G, Joubert D. From ultrasoft pseudopotentials to the projector augmented-wave method. Phys Rev B 1999;59:1758.
[36] Moroni EG, Kresse G, Hafner J, Furthmuller J. Ultrasoft pseudopotentials applied to magnetic Fe, Co, and Ni: from atoms to solids. Phys Rev B 1997;56:15629.
[37] Kittel C. Introduction to solid state physics. 7th ed. New York: Wiley; 1996.
[38] Mclellan RB, Harkins CG. Hydrogen interactions with metals. Mater Sci Eng 1975;18:5–35.
[39] Irikura KK. Experimental vibrational zero-point energies: diatomic molecules. J Phys Chem 2007;36:389–97.
[40] Monkhorst HJ, Pack JD. Special points for Brillouin-zone integrations. Phys Rev B 1976;13:5188.
[41] Methfessel M, Paxton AT. High-precision sampling for Brillouin-zone integration in metals. Phys Rev B 1989;40:3616.

[42] Reuter K, Scheffler M. Composition, structure, and stability of RuO2(110) as a function of oxygen pressure. Phys Rev B 2001;65:035406.
[43] Van de Walle CG, Neugebauer J. Role of hydrogen in surface reconstructions and growth of GaN. J Vac Sci Technol B 2002;20:1640.
[44] Sugimoto H, Fukai Y. Solubility of hydrogen in metals under high hydrogen pressures: thermodynamical calculations. Acta Metall Mater 1992;40:2327.
[45] Hemmes H, Driessen A, Griessen R. Thermodynamic properties of hydrogen at pressures up to 1 Mbar and temperatures between 100 and 1000K. J Phys C 1986;19:3571.
[46] Ji M, Wang CZ, Ho KM, Adhikari S, Hebert KR. Statistical model of defects in Al-H system. Phys Rev B 2010;81:024105.
[47] Philibert J. Atom movements: diffusion and mass transport in solids. France: Les editions de Physique; 1991.
[48] Wert C, Zener C. Interstitial atomic diffusion coefficients. Phys Rev 1949;76:1169.
[49] Wigner EZ. Phys Chem Abt B 1932;19:203.
[50] Wigner E. The transition state method. Trans Faraday Soc 1938;34:29.
[51] Jonsson H, Mills G, Jacobsen KW. Classical and quantum dynamics in condensed phase simulations. New Jersey/ London: World Scientific; 1998. p. 385.
[52] Lu XG, Selleby M, Sundman B. Assessments of molar volume and thermal expansion for selected bcc, fcc and hcp metallic elements. Comput Coupling Phase Diagrams Thermochem 2005;29:68.
[53] Jansson B. TRITA-MAC 0234. Stockholm, Sweden: Royal Institute of Technology; 1984.
[54] Andersson JO, Helander T, Höglund L, Shi P, Sundman B. CALPHAD 2002;26:273.
[55] Ling C, Sholl DS. First-principles evaluation of carbon diffusion in Pd and Pd-based alloys. Phys Rev B 2009;80:214202.
[56] Puska MJ, Nieminen RM, Manninen M. Atoms embedded in an electron gas: immersion energies. Phys Rev B 1981;24:3037.
[57] Liu YL, Zhang Y, Zhou HB, Lu GH, Liu F, Luo G-N. Vacancy trapping mechanism for hydrogen bubble formation in metal. Phys Rev B 2009;79:172103.
[58] Zhou HB, Jin S, Zhang Y, Lu GH, Liu F. Anisotropic strain enhanced hydrogen solubility in bcc metals: the independence on the sign of strain. Phys Rev Lett 2012;109:135502.
[59] Wang Y, Liu ZK, Chen LQ. Thermodynamic properties of Al, Ni, NiAl, and Ni3Al from first-principles calculations. Acta Mater 2004;52:2665.
[60] Togo A, Chaput L, Tanaka I, Hug G. First-principles phonon calculations of thermal expansion in $Ti_3SiC_2$,$Ti_3AlC_2$, and $Ti_3GeC_2$. Phys Rev B 2010;81:174301.
[61] Woo SJ, Lee ES, Yoon M, Kim YH. Finite-temperature hydrogen adsorption and desorption thermodynamics driven by soft vibration modes. Phys Rev Lett 2013;111:066102.
[62] Wimmer E, Wolf W, Sticht J, Saxe P. Temperature-dependent diffusion coefficients from ab initio computations: hydrogen, deuterium, and tritium in nickel. Phys Rev B 2008;77:134305.
[63] Ismer L, Hickel T, Neugebauer J. Ab initio study of the solubility and kinetics of hydrogen in austenitic high Mn steels. Phys Rev B 2010;81:094111.
[64] Yokoyama H, Numakura H, Koiwa M. The solubility and diffusion of carbon in palladium. Acta Mater 1998;46:2823.
[65] Jiang WB, Kong QP, Molodov DA, Gottstein G. Compensation effect in grain boundary internal friction. Acta Mater 2009;57:3327.
[66] Constable FH. Proc Roy Soc 1925;A108:355.
[67] Dienes GJ. Frequency factor and activation energy for the volume diffusion of metals. J Appl Phys 1950;21:1189.